Crystal-field splitting and correlation effect on the electronic structure of A2IrO3

H. Gretarsson, J. P. Clancy, X. Liu, J. P. Hill, Emil Bozin, Yogesh Singh, S. Manni, Philipp Gegenwart, Jungho Kim, A. H. Said, D. Casa, T. Gog, M. H. Upton, Heung-Sik Kim, J. Yu, Vamshi M. Katukuri, L. Hozoi, Jeroen van den Brink, Young-June Kim

Angaben zur Veröffentlichung / Publication details:

Gretarsson, H., J. P. Clancy, X. Liu, J. P. Hill, Emil Bozin, Yogesh Singh, S. Manni, et al. 2013. "Crystal-field splitting and correlation effect on the electronic structure of A2IrO3." *Physical Review Letters* 110 (7): 076402. https://doi.org/10.1103/physrevlett.110.076402.

Crystal-Field Splitting and Correlation Effect on the Electronic Structure of A_2IrO_3

H. Gretarsson,[1] J. P. Clancy,[1] X. Liu,[2] J. P. Hill,[2] Emil Bozin,[2] Yogesh Singh,[3] S. Manni,[4] P. Gegenwart,[4] Jungho Kim,[5] A. H. Said,[5] D. Casa,[5] T. Gog,[5] M. H. Upton,[5] Heung-Sik Kim,[6] J. Yu,[6] Vamshi M. Katukuri,[7] L. Hozoi,[7] Jeroen van den Brink,[7] and Young-June Kim[1,*]

[1]*Department of Physics, University of Toronto, 60 St. George Street, Toronto, Ontario M5S 1A7, Canada*
[2]*CMP&MS Department, Brookhaven National Laboratory, Upton, New York 11973, USA*
[3]*Indian Institute of Science Education and Research Mohali, Sector 81, SAS Nagar, Manauli PO 140 306, Punjab, India*
[4]*I. Physikalisches Institut, Georg-August-Universität Göttingen, D-37077 Göttingen, Germany*
[5]*Advanced Photon Source, Argonne National Laboratory, Argonne, Illinois 60439, USA*
[6]*Department of Physics and Astronomy, Seoul National University, Seoul 151-747, Korea*
[7]*Institute for Theoretical Solid State Physics, IFW Dresden, Helmholtzstrasse 20, 01069 Dresden, Germany*

(Received 21 September 2012; published 13 February 2013)

The electronic structure of the honeycomb lattice iridates Na_2IrO_3 and Li_2IrO_3 has been investigated using resonant inelastic x-ray scattering (RIXS). Crystal-field-split *d-d* excitations are resolved in the high-resolution RIXS spectra. In particular, the splitting due to noncubic crystal fields, derived from the splitting of $j_{\text{eff}} = 3/2$ states, is much smaller than the typical spin-orbit energy scale in iridates, validating the applicability of j_{eff} physics in A_2IrO_3. We also find excitonic enhancement of the particle-hole excitation gap around 0.4 eV, indicating that the nearest-neighbor Coulomb interaction could be large. These findings suggest that both Na_2IrO_3 and Li_2IrO_3 can be described as spin-orbit Mott insulators, similar to the square lattice iridate Sr_2IrO_4.

DOI: 10.1103/PhysRevLett.110.076402 PACS numbers: 71.70.Ej, 75.10.Jm, 75.25.Dk, 78.70.Ck

The intense interest in iridium oxides, or iridates, arises from a number of competing interactions of similar magnitude [1–9]. While the on-site Coulomb interaction is the dominant energy scale in 3*d* transition metal oxides, the spin-orbit coupling (SOC) is largely ignored. On the other hand, for 5*d* elements such as Ir, the SOC becomes significant and in fact plays a dominant role. A good example is Sr_2IrO_4, whose electronic states are well described by $j_{\text{eff}} = 1/2$ states arising from the spin-orbit-split t_{2g} levels [2,3,8].

One of the most intensely scrutinized families of iridates is the honeycomb lattice family A_2IrO_3 (A = Na, Li) [5,7,10–14]. Originally thought of as Mott [4] or topological insulators [5], these materials are now believed to be Mott insulators [10,11]. A recent calculation, though, suggests that uniaxial strain might still drive the system to topological insulating behavior [15]. Furthermore, these materials could be described with the Kitaev-Heisenberg model [7,11,12], in which bond-dependent Kitaev interactions are realized and support various types of topological phases. The applicability of such intriguing theoretical possibilities to a real system crucially depends on the j_{eff} physics arising from strong SOC. However, the experimental situation seems to be far from clear. In particular, structural refinements find a sizable trigonal distortion of the IrO_6 octahedra [16,17], which will produce crystal-field splittings within the t_{2g} manifold. If the splitting is comparable to the SOC, the $j_{\text{eff}} = 1/2$ states will mix with $j_{\text{eff}} = 3/2$ states [18] and the relevant microscopic model becomes quite different from the ideal j_{eff} physics [14,19], preventing the Kitaev-Heisenberg model from being realized [7,11,13]. Recent theoretical studies have even suggested that the ground state has a large contribution from the $j_{\text{eff}} = 3/2$ state [20].

Therefore, it is of great importance to elucidate the underlying electronic structure of Na_2IrO_3 experimentally. In particular, the spectroscopic investigation of excitations between spin-orbit-split j_{eff} states can provide us with direct information regarding the size of the crystal-field splitting with respect to the typical SOC energy scale in iridates (0.4–0.5 eV) [21,22]. In the case of Sr_2IrO_4, such excitations from $j_{\text{eff}} = 3/2$ to $j_{\text{eff}} = 1/2$ were observed around 0.6–0.8 eV in the resonant inelastic x-ray scattering (RIXS) data [8], which are accounted for in the quantum chemical calculation by Katukuri *et al.* [23]. The splitting within these "spin-orbit" excitations arises due to nonzero tetragonal crystal fields and is much smaller (~ 0.1 eV) than the SOC, justifying the j_{eff} description of Sr_2IrO_4.

In this Letter, we present a comprehensive picture of the low energy electronic structure of Na_2IrO_3 and Li_2IrO_3, based on Ir L_3-edge RIXS experiments. Our high-resolution RIXS measurements allow us to resolve the crystal-field splitting of the $j_{\text{eff}} = 3/2$ states due to the trigonal distortion, which is determined to be about 110 meV in both compounds. This energy scale agrees very well with quantum chemical calculations and is much smaller than the typical value for SOC, validating the j_{eff} picture in these compounds. We have also studied the momentum dependence of the insulating gap; the observed flat dispersion of the insulating gap is consistent

with what is expected from a significant Coulomb interaction in both compounds. Taken together, we argue that, just as Sr_2IrO_4, the honeycomb A_2IrO_3 iridates can be described as spin-orbit Mott insulators [2,15,19,24].

The RIXS experiment was carried out at the Advanced Photon Source using the 30ID MERIX and the 9ID RIXS spectrometer. A spherical (1 m radius) diced Si(844) analyzer and a Si(844) secondary monochromator were used to obtain the overall energy resolution (FWHM) of ~35 meV [25]. To minimize the elastic background, most of the measurements were carried out in a horizontal scattering geometry near $\mathbf{Q} = (0\,0\,6.7)$, for which the scattering angle 2θ was close to 90°. We use the $C2/m$ notation for the lattice [16,17]. A single crystal of Na_2IrO_3 and a polycrystalline sample of Li_2IrO_3 were grown by the solid-state synthesis method, previously described in detail [10,11]. The Na_2IrO_3 crystal was platelike with a flat shiny surface; the surface normal was in the (001) direction.

The RIXS process at the L_3 edge of Ir (or any other d electron system) is a second order process consisting of two dipole transitions ($2p \rightarrow 5d$ followed by $5d \rightarrow 2p$). Therefore, it is especially valuable for detecting excitations between the d levels and has been extensively utilized in the study of $3d$ transition metal compounds [26–32]. Recent instrumental advances have made it possible to measure collective magnetic excitations [8,33]. In A_2IrO_3, Ir^{4+} ions are in the $5d^5$ configuration in a slightly distorted octahedral environment of oxygen ions, with the edge-sharing IrO_6 octahedra forming a honeycomb net. Due to the octahedral crystal field, there exists a fairly large splitting ($10Dq$) between the t_{2g} and e_g states. Since the $5d$ orbitals are spatially more extended than the $3d$ orbitals, the $10Dq$ value is expected to be much larger. Indeed, in our RIXS investigations of various iridium compounds, well-separated t_{2g} and e_g states have been observed, with the $10Dq$ value typically about 3 eV [34].

In Fig. 1, a representative high-resolution RIXS spectrum of Na_2IrO_3 is plotted on a wide energy scale. This scan was obtained at room temperature and plotted as a function of energy loss ($\hbar\omega = E_i - E_f$). The incident energy, $E_i = 11.217$ keV, was chosen to maximize the resonant enhancement of the spectral features of interest below 1 eV. A broad and strong feature is observed at 2–4 eV, and other sharper features are observed below 1 eV, corresponding to d-d transitions from occupied t_{2g} states into the empty e_g and t_{2g} levels, respectively. Also plotted in the figure are the room temperature data of polycrystalline Li_2IrO_3. A lack of significant momentum dependence of these d-d excitations (shown later in Fig. 2) allows one to directly compare the peak positions between the single crystal and powder samples. The spectra were fit to five peaks (labeled A-E), as shown by the dashed black lines. The low energy excitations can be fit to three peaks, two Gaussians (B and C) of the same width and one Lorentzian peak (A) on top of a broad background (Gaussian). Two

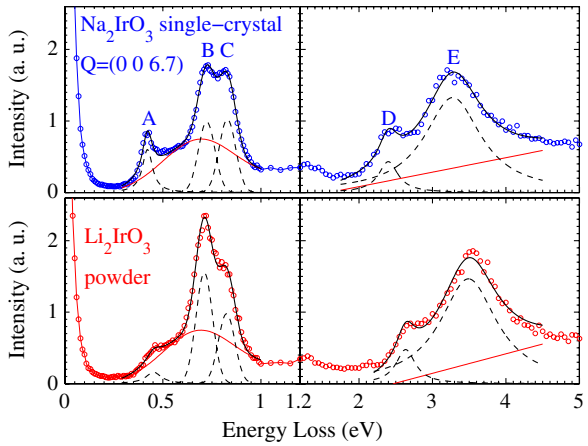

FIG. 1 (color online). Top: Wide energy range RIXS spectrum for a single-crystal sample of Na_2IrO_3 at $\mathbf{Q} = (0\,0\,6.7)$ obtained with $E_i = 11.217$ keV. Note the different scale used for the left and right panels. Bottom: RIXS spectrum for the Li_2IrO_3 powder sample at $|\mathbf{Q}| \approx 8$ Å^{-1}, obtained with the same E_i. All spectra were measured at room temperature. The dashed black curves are the result of a fit (see the text), and the thin solid red lines represent the background.

Lorentzian functions with sloping background were used to fit the higher energy excitations (D and E). The resulting peak positions are listed in Table I.

To clarify the nature of the excitations revealed by RIXS, we have carried out multiconfiguration self-consistent-field and multireference configuration-interaction (MRCI) calculations [35] on clusters consisting of one central IrO_6 octahedron, all adjacent Na or Li ions, and the three nearest-neighbor IrO_6 octahedra (see Ref. [23] and the Supplemental Material [36] for details). Local d-d transitions are computed only for the central IrO_6 octahedron, while the nearest-neighbor octahedra are explicitly included in the cluster for providing an accurate description of the nearby charge distribution. Two different lattice configurations are considered: i.e., the $C2/c$ structure [10,37] and also the $C2/m$ arrangement proposed more recently [16,17,38].

The results of the spin-orbit MRCI (MRCI + SOC) calculations using the $C2/m$ configuration [16] are listed for Na_2IrO_3 in the third column of Table I. The MRCI + SOC data fit the experiment reasonably well, with peaks B and C corresponding to $j_{\text{eff}} = 3/2$ to $j_{\text{eff}} = 1/2$ electronic transitions. Above 2.5 eV, the MRCI + SOC results indicate multiple t_{2g} to e_g excitations displaying a two-peak structure reminiscent of the D and E features in the RIXS spectra. Although direct comparison is difficult due to the broad spectral widths of D and E arising from multiple excitations, MRCI + SOC seems to overestimate somewhat the relative energies of those latter features. Interestingly, for the alternative $C2/c$ structure of Na_2IrO_3 [10], the splitting between the two doublets originating from the $j_{\text{eff}} = 3/2$ quartet is much larger and the position of the

TABLE I. RIXS and MRCI + SOC excitation energies ($C2/m$ structure) for 213 iridates (eV).

	Na213 RIXS	Na213 MRCI	Li213 RIXS	Li213 MRCI
Peak A	0.42(1)	⋯	0.45(2)	⋯
Peak B	0.72(2)	0.82	0.72(2)	0.80
Peak C	0.83(2)	0.89	0.83(2)	0.97
Peak D	2.4(1)	2.8–3.4	2.6(1)	3.1–3.7
Peak E	3.3(1)	3.8–4.1	3.5(1)	4.1–5.0

C peak is overestimated by 0.25 eV in the MRCI + SOC treatment. Since the deviations from the experimental data are in this case larger, the MRCI + SOC results for $C2/c$ symmetry are not listed in Table I. The t_{2g} splittings in calculations with no SOC are in fact as large as 0.6 eV for the $C2/c$ structure of Na_2IrO_3, which gives rise to a highly uneven admixture of t_{2g} components in the spin-orbit calculations. In contrast, for the $C2/m$ configuration, the t_{2g} splittings are about 0.1 eV and the three different t_{2g} hole configurations contribute with similar weight to the spin-orbit ground-state wave function (see Table II).

For Li_2IrO_3, the calculations correctly reproduce the shift to higher energies of the t_{2g} to e_g transitions relative to those in Na_2IrO_3. The discrepancy between the experimental values and the MRCI + SOC results (e.g., peak C) could be caused by the uncertainty in the structural model used for this calculation ($C2/m$ from Ref. [38]). Since local structural disorder is not easily captured in the regular diffraction data, local structure probes such as pair-distribution-function (PDF) measurements can sometimes be useful for clarifying the structural details. We have carried out x-ray PDF studies on Li_2IrO_3 and Na_2IrO_3 powder samples. Details of these measurements and the comparison of the two structures are reported in the Supplemental Material [36]. Except for the overall lattice contraction, the Li_2IrO_3 PDF seems to be well described by the $C2/m$ symmetry, eliminating the local structural disorder as a possible explanation. The most likely cause of the structural uncertainty is the oxygen position, since x-ray structural probes are not particularly sensitive to light elements like oxygen [37,38]. We note that the latest refinements using both powder neutron and single-crystal x-ray data on Na_2IrO_3 do show important differences compared to earlier x-ray powder diffraction data and that the MRCI + SOC results are very different for the two structures. Better structural refinements using neutron diffraction would reduce the oxygen position uncertainty in Li_2IrO_3 and could improve the agreement between our MRCI + SOC calculation and the experiment.

TABLE II. Percentage contributions of the different Ir $5d^5$ configurations to the lowest on-site d-d excited states in Na_2IrO_3, as obtained from MRCI + SOC calculations.

Energy (eV)	0	0.82	0.89
$d^2_{xy}d^2_{yz}d^1_{zx}$	38.7	24.3	32.2
$d^2_{xy}d^1_{yz}d^2_{zx}$	34.7	60.3	24.7
$d^1_{xy}d^2_{yz}d^2_{zx}$	26.6	15.4	43.1

One of our main findings is that the splitting of the strong RIXS peak located at 0.7–0.8 eV is due to the trigonal distortion which is well corroborated with our MRCI + SOC calculations. The fact that this splitting (110 meV) is much smaller than a SOC of 0.4–0.5 eV [21,22] strongly supports that these excitations are transitions from crystal-field-split $j_{\text{eff}} = 3/2$ levels to the $j_{\text{eff}} = 1/2$ state (labeled as a spin-orbit exciton in Ref. [8]). Given that the optical gap in this material is about 350 meV [24] and that there is no such excitation in the MRCI + SOC calculations, which only look at on-site d-d excitations, it is reasonable to associate feature A at low energy as arising from the excitation of a particle and hole pair across the charge gap. Additional periodic density functional theory (DFT) calculations using generalized-gradient approximations (GGA) show that a moderate size U and SOC can indeed open a (Mott) gap of 300–400 meV, in accordance with the experimental observation (see the Supplemental Material [36]).

The nature of the charge excitation gap can be further revealed by its momentum dependence. In Fig. 2, we plot the momentum dependence of the low energy peaks (A-C) in Na_2IrO_3. In the honeycomb plane, the magnetic ordering doubles the unit cell [39], and correspondingly the first Brillouin zone (BZ) becomes smaller. Two different BZ schemes are illustrated in the inset of Fig. 2(a) to aid the comparison. We will use the rectangular BZ notation. Note that the two high symmetry directions of interest, the $\mathbf{q} = (h\ 0)$ and $\mathbf{q} = (0\ k)$ in rectangular notation, correspond to the Γ-K and Γ-M directions in the honeycomb plane, respectively. One can see that the overall momentum dependence of the excitation spectrum is very small, except for peak A. To investigate the behavior of peak A in detail, the low energy portion of the spectra was fit to a Lorentzian peak. Since the peak seems to disappear at $\mathbf{q} = (1\ 0)$, we have used the spectrum at this $\mathbf{q}$ as an empirical background. The fitting results for peak positions, widths, and intensities are shown in Figs. 2(b) and 2(c). The width and peak position remain almost unchanged (≈ 10 meV dispersion), but the intensity is strongly peaked around the BZ center. This can be clearly seen in the pseudocolor plot of the spectra shown in Fig. 2(d), in which a strong peak around $\mathbf{q} = (0\ 0)$ and 0.42 eV is contrasted with the $\mathbf{q}$-independent features $B + C$. In addition, one can see that the spectral weight changes abruptly around 0.4 eV, confirming that this is the particle-hole continuum boundary. Based on our RIXS results, the electronic excitations in A_2IrO_3 can be summarized, as is shown in Fig. 2(e).

It is clear from this observation that the insulating gap is direct (minimum gap at Γ). The relatively flat dispersion

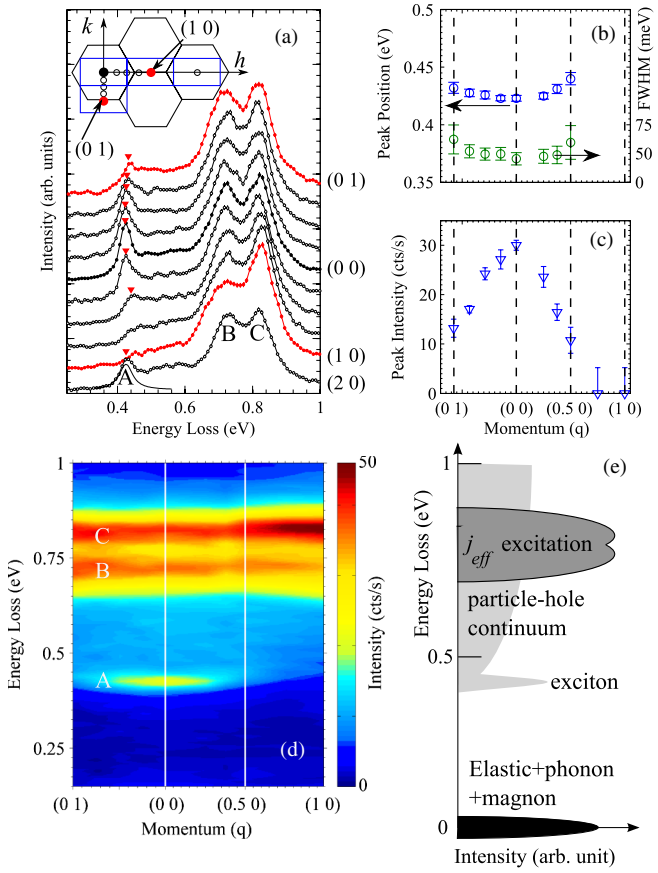

FIG. 2 (color online). (a) Momentum dependence of the low energy RIXS spectra of Na_2IrO_3 obtained at $T = 9$ K. The inset shows a schematic diagram of the (h k 0) reciprocal space plane. The BZs corresponding to the monoclinic unit cell are blue rectangles. For comparison, we also plot the BZ of the honeycomb net in black. The circles are the points where RIXS spectra are taken. The low energy peaks denoted with red triangles are fit to a Lorentzian, and the momentum dependence of (b) the peak position and width and (c) the peak intensity are shown. (d) The same data are plotted in a false color scale. (e) Schematics of electronic excitations in A_2IrO_3 determined from our RIXS measurements.

observed in our data is also consistent with the DFT calculation, which suggests that the bandwidth is about 50% (40%) for the GGA + SOC (GGA + SOC + U) result compared to the GGA-only case, leading to an almost dispersionless charge gap. Both the sharpness in energy and the momentum dependence of peak A are quite reminiscent of the excitonic behavior of the BZ center particle-hole excitation across the charge-transfer gap in the insulating cuprate La_2CuO_4 [40]. This suggests that an extra nearest-neighbor Coulomb interaction V (in addition to the on-site interaction U) might be important for modeling this material [41,42]. Sizable V could promote the tendency toward exciton binding and also further narrow the bandwidths. The smaller intensity of the charge gap feature in Li_2IrO_3 compared to Na_2IrO_3 could be due to the fact that the Li_2IrO_3 data are powder averaged. However, one cannot rule out the possibility of weaker V in Li_2IrO_3 as compared to Na_2IrO_3.

Another interesting aspect of our data is that the dispersion of the gap appears to follow the underlying honeycomb lattice rather than the crystallographic or magnetic unit cell. This is clearly observed by the spectrum obtained at $\mathbf{q} = (2\ 0)$. While (2 0) is the next BZ center along the Γ-K direction (in honeycomb notation), (1 0) is on the zone boundary; peak A disappears at (1 0) but recovers its intensity at the $\mathbf{q} = (2\ 0)$ position. Additional momentum dependence data, reported in the Supplemental Material [36], show the lack of momentum dependence along the L direction (perpendicular to the honeycomb plane). Therefore, the electronic structure of Na_2IrO_3 seems to be quite well described as that of a 2D honeycomb lattice.

It is worth comparing the observed low energy RIXS spectrum with that of Sr_2IrO_4. In Sr_2IrO_4, a low energy magnon was observed below 200 meV, while highly dispersive excitations were observed between 0.4 and 0.8 eV. This latter band of excitations is composed of particle-hole excitation across the Mott gap and spin-orbit excitations from the $j_{\rm eff} = 3/2$ to the $j_{\rm eff} = 1/2$ states. Because of the smaller single-particle bandwidth in A_2IrO_3 (see the DFT calculations in Ref. [15]), the "$j_{\rm eff}$ excitation" in Na_2IrO_3 is almost dispersionless, unlike the highly dispersive counterpart in Sr_2IrO_4. Perhaps an even more significant difference is the well-separated energy scale of the $j_{\rm eff}$ excitation and the particle-hole continuum in Na_2IrO_3. These two energy scales are very similar in Sr_2IrO_4, but the large separation in Na_2IrO_3 allows one to investigate these two types of excitation separately.

To summarize, we have carried out resonant inelastic x-ray scattering investigations of electronic excitations in Na_2IrO_3 and Li_2IrO_3. We observe three well-defined features below 1 eV and a broad two-peak feature at 2–5 eV. By comparing our observation with quantum chemical and density functional theory calculations, we associate these features with d-d transitions. Specifically, the high energy excitations are from t_{2g} to e_g excitations, while the low energy excitations around 0.7–0.8 eV are excitations from $j_{\rm eff} = 3/2$ to $j_{\rm eff} = 1/2$ states. The splitting of the latter feature arising from the trigonal crystal field is about 110 meV, much smaller than the spin-orbit-coupling energy scale of Ir compounds, which validates the applicability of $j_{\rm eff}$ physics in A_2IrO_3. In addition, we observe a lower energy excitation around 0.4 eV, which shows very little momentum dependence and is associated with the particle-hole excitation across the Mott gap; the "excitonic" behavior of this peak suggests the nearest-neighbor Coulomb interaction V is sizable. We conclude that the electronic structures of both Na_2IrO_3 and Li_2IrO_3 are similar and that these systems can be described as spin-orbit Mott insulators.

We would like to thank Y. B. Kim and S. Bhattacharjee for fruitful discussions and Doug Robinson for technical assistance during the PDF measurements. Research at the University of Toronto was supported by the NSERC, CFI, and OMRI. This research benefited from the RIXS Collaboration, which is supported by the Computational Materials and Chemical Sciences Network (CMCSN) Program of the Division of Materials Science and Engineering, U.S. Department of Energy, Grant No. DE-SC0007091. Use of the APS was supported by the U.S. DOE Office of Science, under Contract No. DE-AC02-06CH11357. Work performed at Brookhaven National Laboratory was supported by the DOE, Office of Science, Division of Materials Science, under Contract No. DE-AC02-98CH10886. Y.-J. Kim was supported by the KOFST through the Brainpool Program. H.-S. Kim and J. Yu were supported by the NRF through the ARP (R17-2008-033-01000-0). H.-S. Kim would like to acknowledge the support from the KISTI Supercomputing Center through the strategic support program for supercomputing application research (No. KSC-2010-S00-0005). S. Manni acknowledges support from the Erasmus Mundus Eurindia Project.

*yjkim@physics.utoronto.ca

[1] Y. Okamoto, M. Nohara, H. Aruga-Katori, and H. Takagi, Phys. Rev. Lett. **99**, 137207 (2007).
[2] B. J. Kim *et al.*, Phys. Rev. Lett. **101**, 076402 (2008).
[3] B. J. Kim, H. Ohsumi, T. Komesu, S. Sakai, T. Morita, H. Takagi, and T. Arima, Science **323**, 1329 (2009).
[4] G. Jackeli and G. Khaliullin, Phys. Rev. Lett. **102**, 017205 (2009).
[5] A. Shitade, H. Katsura, J. Kuneš, X.-L. Qi, S.-C. Zhang, and N. Nagaosa, Phys. Rev. Lett. **102**, 256403 (2009).
[6] D. Pesin and L. Balents, Nat. Phys. **6**, 376 (2010).
[7] J. Chaloupka, G. Jackeli, and G. Khaliullin, Phys. Rev. Lett. **105**, 027204 (2010).
[8] J. Kim *et al.*, Phys. Rev. Lett. **108**, 177003 (2012).
[9] J. P. Clancy, N. Chen, C. Y. Kim, W. F. Chen, K. W. Plumb, B. C. Jeon, T. W. Noh, and Y.-J. Kim, Phys. Rev. B **86**, 195131 (2012).
[10] Y. Singh and P. Gegenwart, Phys. Rev. B **82**, 064412 (2010).
[11] Y. Singh, S. Manni, J. Reuther, T. Berlijn, R. Thomale, W. Ku, S. Trebst, and P. Gegenwart, Phys. Rev. Lett. **108**, 127203 (2012).
[12] J. Chaloupka, G. Jackeli, and G. Khaliullin, arXiv:1209.5100v1.
[13] J. Reuther, R. Thomale, and S. Trebst, Phys. Rev. B **84**, 100406(R) (2011).
[14] I. I. Mazin, H. O. Jeschke, K. Foyevtsova, R. Valentí, and D. I. Khomskii, Phys. Rev. Lett. **109**, 197201 (2012).
[15] C. H. Kim, H. S. Kim, H. Jeong, H. Jin, and J. Yu, Phys. Rev. Lett. **108**, 106401 (2012).
[16] S. K. Choi *et al.*, Phys. Rev. Lett. **108**, 127204 (2012).
[17] F. Ye, S. Chi, H. Cao, B. C. Chakoumakos, J. A. Fernandez-Baca, R. Custelcean, T. F. Qi, O. B. Korneta, and G. Cao, Phys. Rev. B **85**, 180403 (2012).
[18] X. Liu *et al.*, Phys. Rev. Lett. **109**, 157401 (2012).
[19] S. Bhattacharjee, S.-S. Lee, and Y. B. Kim, New J. Phys. **14**, 073015 (2012).
[20] S. W. Lovesey and A. N. Dobrynin, J. Phys. Condens. Matter **24**, 382201 (2012).
[21] B. Andlauer, J. Schneider, and W. Tolksdorf, Phys. Status Solidi B **73**, 533 (1976).
[22] K. W. Blazey and F. Levy, Solid State Commun. **59**, 335 (1986).
[23] V. M. Katukuri, H. Stoll, J. van den Brink, and L. Hozoi, Phys. Rev. B **85**, 220402 (2012).
[24] R. Comin *et al.*, Phys. Rev. Lett. **109**, 266406 (2012).
[25] Y. J. Kim, J. P. Hill, J. Kim, and D. Casa, Synchrotron Radiation News **25**, 3 (2012).
[26] M. M. Sala *et al.*, New J. Phys. **13**, 043026 (2011).
[27] G. Ghiringhelli, M. Matsubara, C. Dallera, F. Fracassi, A. Tagliaferri, N. Brookes, A. Kotani, and L. Braicovich, Phys. Rev. B **73**, 035111 (2006).
[28] A. Uldry, F. Vernay, and B. Delley, Phys. Rev. B **85**, 125133 (2012).
[29] G. Ghiringhelli, N. Brookes, E. Annese, H. Berger, C. Dallera, M. Grioni, L. Perfetti, A. Tagliaferri, and L. Braicovich, Phys. Rev. Lett. **92**, 117406 (2004).
[30] L. J. P. Ament, M. van Veenendaal, T. P. Devereaux, J. P. Hill, and J. van den Brink, Rev. Mod. Phys. **83**, 705 (2011).
[31] M. Z. Hasan, E. D. Isaacs, Z. X. Shen, L. L. Miller, K. Tsutsui, T. Tohyama, and S. Maekawa, Science **288**, 1811 (2000).
[32] J. Schlappa, K. Wohlfeld, K. J. Zhou, M. Mourigal, M. W. Haverkort, V. N. Strocov, L. Hozoi, C. Monney, S. Nishimoto, S. Singh *et al.*, Nature (London) **485**, 82 (2012).
[33] L. Braicovich *et al.*, Phys. Rev. Lett. **102**, 167401 (2009).
[34] H. Gretarsson, J. Kim, D. Casa, T. Gog, K. R. Choi, S. W. Cheong, and Y.-J. Kim, Phys. Rev. B **84**, 125135 (2011).
[35] T. Helgaker, P. Jørgensen, and J. Olsen, *Molecular Electronic-Structure Theory* (Wiley, Chichester, 2000).
[36] See Supplemental Material at http://link.aps.org/supplemental/10.1103/PhysRevLett.110.076402 for detailed description of the electronic structure and quantum chemical calculations, additional RIXS spectra, and PDF experiments.
[37] H. Kobayashi, M. Tabuchi, M. Shikano, H. Kageyama, and R. Kanno, J. Mater. Chem. **13**, 957 (2003).
[38] M. J. O'Malley, H. Verweij, and P. M. Woodward, J. Solid State Chem. **181**, 1803 (2008).
[39] X. Liu, T. Berlijn, W.-G. Yin, W. Ku, A. Tsvelik, Y.-J. Kim, H. Gretarsson, Y. Singh, P. Gegenwart, and J. P. Hill, Phys. Rev. B **83**, 220403 (2011).
[40] D. S. Ellis, J. Hill, S. Wakimoto, R. Birgeneau, D. Casa, T. Gog, and Y.-J. Kim, Phys. Rev. B **77**, 060501 (2008).
[41] J. van den Brink, M. B. J. Meinders, J. Lorenzana, R. Eder, and G. A. Sawatzky, Phys. Rev. Lett. **75**, 4658 (1995).
[42] R. Neudert, M. Knupfer, M. S. Golden, J. Fink, W. Stephan, K. Penc, N. Motoyama, H. Eisaki, and S. Uchida, Phys. Rev. Lett. **81**, 657 (1998).